NANO LETTERS

Letter

pubs.acs.org/NanoLett

Dynamical Evolution of Anisotropic Response in Black Phosphorus under Ultrafast Photoexcitation

Shaofeng Ge,[†,‡] Chaokai Li,[†,‡] Zhiming Zhang,[†,‡] Chenglong Zhang,[†,‡] Yudao Zhang,[†,‡] Jun Qiu,[†,‡] Qinsheng Wang,[†,‡] Junku Liu,[†,§] Shuang Jia,[†,‡] Ji Feng,*[,†,‡] and Dong Sun*[,†,‡]

[†]International Center for Quantum Materials, School of Physics, Peking University, Beijing 100871, People's Republic of China

[‡]Collaborative Innovation Center of Quantum Matter, Beijing 100871, People's Republic of China

[§]Qian Xuesen Laboratory of Space Technology, China Academy of Space Technology, Beijing 100094, People's Republic of China

Supporting Information

ABSTRACT: Black phosphorus has recently emerged as a promising material for high-performance electronic and optoelectronic device for its high mobility, tunable mid-infrared bandgap, and anisotropic electronic properties. Dynamical evolution of photoexcited carriers and the induced transient change of electronic properties are critical for materials' high-field performance but remain to be explored for black phosphorus. In this work, we perform angle-resolved transient reflection spectroscopy to study the dynamical evolution of anisotropic properties of black phosphorus under photoexcitation. We find that the anisotropy of reflectivity is enhanced in the pump-induced quasi-equilibrium state, suggesting an extraordinary enhancement of the anisotropy in dynamical conductivity in hot carrier dominated regime. These results raise attractive possibilities of creating high-field, angle-sensitive electronic, optoelectronic, and remote sensing devices exploiting the dynamical electronic anisotropy with black phosphorus.

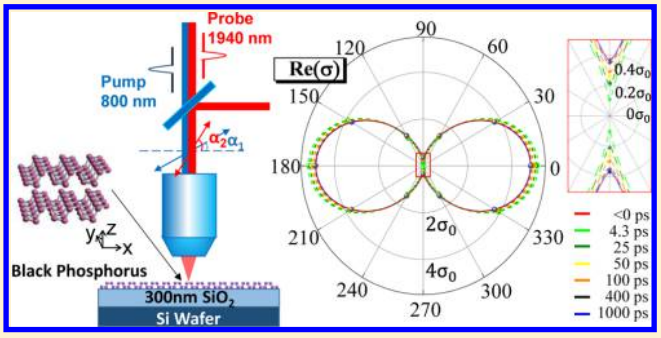

KEYWORDS: *Black phosphorus, two-dimensional materials, ultrafast spectroscopy, electronic anisotropy, high field transport, hot carriers*

As a bridge two-dimensional (2D) material between graphene and transition metal dichalcogenide in terms of mobility and bandgap opening,[1,2] black phosphorus (BP) processes relatively high mobility (up to 50 000 cm/(V s))[3−5] and thickness-dependent bandgap ranging from near-infrared (single layer) to mid-infrared (bulk).[6−8] All these fascinating properties make BP highly promising for applications such as high speed electronic device with high on−off ratio[9−13] and mid-infrared optoelectronics device with low noise.[2,14−19] In addition to these attractive properties, BP also exhibits unusual anisotropic in-plane conductivities resulting from orthorhombic lattice symmetry, which allows for a new degree of freedom in designing conceptually novel optoelectronic, electronic, and optomechanical devices that exploit electronic anisotropy.[2,5,6,15,19−22] Indeed, this electronic anisotropy affords novel device paradigm impossible in graphene and transition metal dichalcogenide. To facilitate device design based on this novel paradigm, the anisotropic steady-state response of BP has been recently investigated using many angle-resolved characterization techniques, such as transmission spectroscopy,[2,7,19] Raman spectroscopy,[2,6] photoconductivity measurement,[2] and photoluminescence measurement.[6] While steady-state transport is governed by the carriers near the Fermi level, transport in high speed devices is determined by the dynamic conductivity of hot carriers, that is, electrons whose temperature is elevated above the lattice temperature due to the presence of high fields and/or dynamic fields in the material.[23,24] Despite its importance for high-performance device, the dynamical anisotropic response of BP under high field has yet to be investigated.

In this work, we performed angle-resolved pump−probe reflection spectroscopy to study the dynamical response of BP in the presence of photoexcitation of hot carriers. The optical excitation with ultrafast pump pulse mimics the working environment of optoelectronic and electronic device operating in the presence of high-field and/or dynamic field. In this regime, carriers are accelerated to elevated energy state, and thus the excited carriers in quasi-equilibrium distributions dominate the device performances. For example, in a typical high speed Si-based device with velocity saturation of 2×10^7 cm/s, the carrier energy is elevated by up to 0.1 eV.[25,26] Therefore, it is interesting to examine the dynamical response of BP under photoexcitation, especially the evolution of electronic anisotropy, through polarization-resolved transient

Received: April 11, 2015
Revised: May 16, 2015
Published: June 3, 2015

DOI: 10.1021/acs.nanolett.5b01409
Nano Lett. 2015, 15, 4650−4656

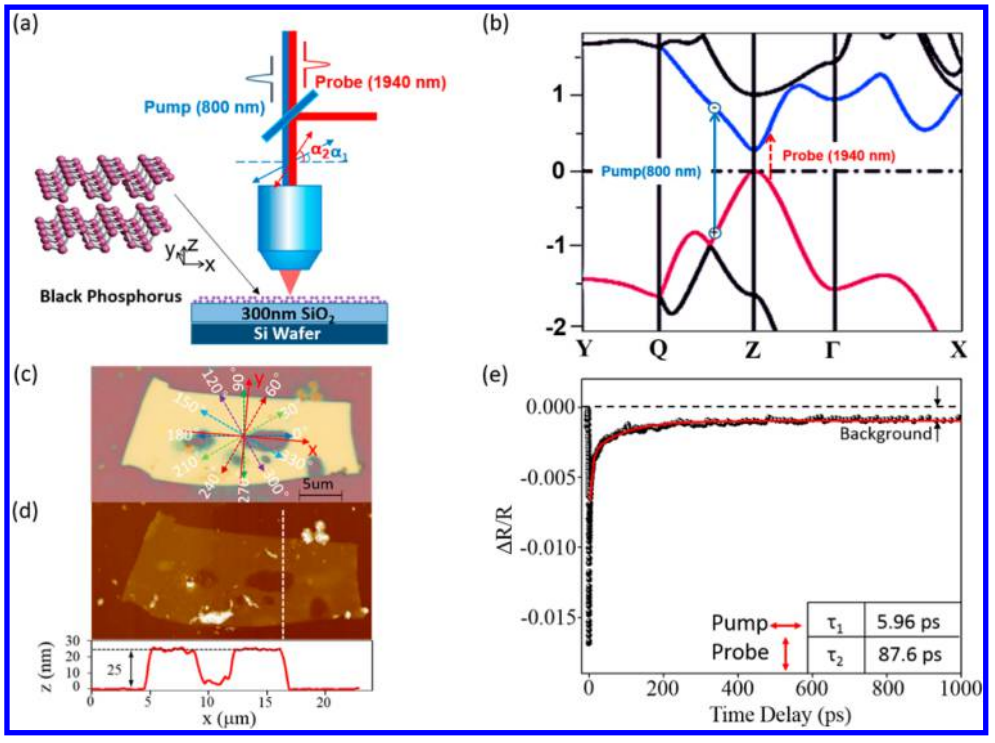

Figure 1. Experimental scheme and sample characterization. (a) Schematic diagram of polarization-resolved transient reflection experiment. (b) Band diagram of black phosphorus and pump (blue) probe (red) photon transition configuration. (c) Optical micrograph, (d) atomic force micrograph, (e) representative transient reflection spectrum with pump polarization along 0° (~x-direction in panel c) and probe polarization at 90° (~y-direction in panel c). The data is fitted by biexponential decay function with two decay time constants: τ_1, τ_2.

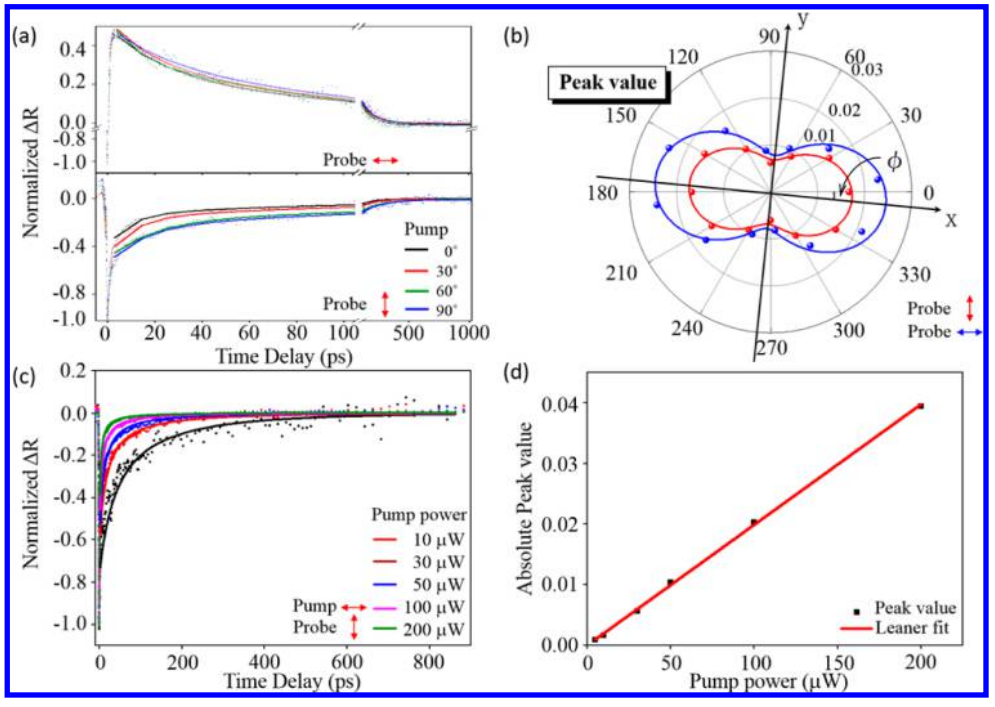

Figure 2. Pump polarization and fluence dependence of transient reflection spectra. (a) Transient reflection spectrum (normalized) with pump laser polarization at 0, 30, 60, and 90° with probe polarization fixed along 0 and 90°. The pump wavelength is 800 nm and the probe wavelength is 1940 nm. The results are fitted by the biexponential decay function. To compare the decay dynamics, the results are normalized by their negative peak values. (b) $\Delta R/R|_{t=0}$ as a function of pump polarization with probe polarization fixed at 0° (blue dots) and 90° (red dots). The polarization dependence of $\Delta R/R|_{t=0}$ can be fit by the function $A_1\cos^2(\theta + \varphi) + A_2\sin^2(\theta + \varphi)$ where φ is the angle between the crystal x direction and the 0° as marked in Figure 1c. The fitting gives the $\varphi = -5.2°$ for probe polarization at 0 and $-5.3°$ for probe polarization at 90°. (c) Normalized ΔR with different pump excitation power (pump polarization of 0° and probe polarization of 90°). (d) $\Delta R/R|_{t=0}$ as a function of pump power. The red line is the leaner fit.

DOI: 10.1021/acs.nanolett.5b01409
Nano Lett. 2015, 15, 4650−4656

reflection measurements. The most remarkable finding inferred from the dynamics of differential reflectance of BP is that not only the anisotropic response of BP is preserved but also the degree of anisotropy is enhanced in the quasi-equilibrium excited states of a high-field device. By systematically varying the combination of pump and probe polarizations, it is revealed that the enhancement of electronic anisotropy in photoexcited quasi-equilibrium states is very robust and largely independent of the polarization of the pump photoexcitation. The anisotropic stretch of the conductivity persists until the hot carriers relax via isotropic cooling and recombination.

As shown in Figure 1a, bulk BP is a layered material with orthorhombic crystal structure.[27] In contrast to graphene, each layer in BP has puckered lattice structure that results in its unique angle-dependent in-plane conductivities[2] due to reduced symmetry. Optical micrograph of a typical thin BP flake is shown in Figure 1c. The majority of later measurements presented in this work are performed on a sample with thickness of 25 nm determined by atomic force microscopy (Figure 1d), from which we can deduce the thickness to be about 47 layers using a layer spacing of 0.53 nm[7]. The as-synthesized BP is found to be p-doped with doping density of $4.2 \times 10^{18}/\mathrm{cm}^3$ by Hall measurement, equivalent to $1.05 \times 10^{13}/\mathrm{cm}^2$ for a 25 nm thick sample ($2 \times 10^{11}/\mathrm{cm}^2$ for each BP layer). Polarization-resolved transient reflection measurement is performed on samples with thickness ranging from 10 to 30 nm in this work and the results are qualitatively similar.

A schematic diagram of the experiment is shown in Figure 1a. A 1.55 eV linear polarized pump laser is used to induce photocarriers in BP. Typical pump fluence is 3×10^{15} photons/cm^2 which converts to $3 \times 10^{14}/\mathrm{cm}^2$ electron–hole pairs at the initial stage using a 0.4%/nm absorption rate at 800 nm[7]. The photoexcited carriers cause quasi-Fermi level shift of 354 meV in conduction band and 225 meV in valence band from a steady state band filling consideration assuming no Fermi level smearing (0 K) in the sample. Because of the photoexcitation, the anisotropic optical conductivity of BP is expected to be modified. To measure dynamical evolution of the anisotropic optical conductivity, polarization resolved 647 meV probe photon arriving at various delay time (t) with respect to pump pulse is used with which the pump induced reflection change (ΔR) is measured. The probe photon energy is only 340 meV larger than the bandgap,[8] which corresponds primarily to the transition involving lowest conduction and highest valence band. The probe polarization is rotatable by a half wave plate, so the anisotropic response of BP can be determined dynamically with a 200 fs time resolution as limited by the convolution of pump–probe pulse.

Figure 1e shows a typical transient reflection spectrum with pump and probe polarization set at 0° and 90°, respectively (angle defined in Figure 1c). The initial $\Delta R/R|_{t=0}$ is negative, which indicates that pump-induced reflection decreases. Subsequently, $\Delta R/R$ decays gradually. However, $\Delta R/R$ reaches a nonzero constant negative value that persists for well beyond 1 ns after the initial pump. This long-lived background is due to elevation of lattice temperature, and the relaxation of this background is attributed to the cooling of lattice temperature of BP through dissipation of heat to the substrate (see Supporting Information). In later analysis, we have subtracted the constant background from $\Delta R/R$.

Figure 2a shows the pump polarization-dependent transient reflection spectra (normalized at $\Delta R/R|_{t=0}$) with probe polarization fixed along 0° and 90°. The transient reflection at time zero ($\Delta R/R|_{t=0}$) shows obvious pump polarization dependence. If we assume $\Delta R/R|_{t=0}$ has linear dependence on photoexcited carrier density, we can simply fit $\Delta R/R|_{t=0}$ as a function of pump polarization angle α_1 (respective to x-axis as marked in Figure 1c) with polarization dependent absorption coefficient A (see Supporting Information for derivation)[7]

$$A \approx \frac{4\sqrt{\varepsilon_1}\left(\mathrm{Re}(\sigma_{xx})\cos^2(\alpha_1) + \mathrm{Re}(\sigma_{yy})\sin^2(\alpha_1)\right)}{\varepsilon_0 c\left(\sqrt{\varepsilon_2} + \sqrt{\varepsilon_1}\right)^2} \quad (1)$$

Here we assume BP layers are sandwiched between two dielectric media, that is, substrate and air, with dielectric constant of ε_1 and ε_2, where σ_{xx} and σ_{yy} are nonzero diagonal component of optical conductivity tensor, ε_0 is the free-space permittivity, and c is the speed of light. The fitting result is shown in Figure 2b, and we can determine the angle between the x-crystal axis of BP and the blue arrow (0° in Figure 1c) to be −5.3°. Similar fitting can be performed on $\Delta R/R|_{t=0}$ with probe polarization fixed along 0°, which gives the same angle of x-crystal axis of BP. The linear dependence of $\Delta R/R|_{t=0}$ on photoexcited carrier density is verified by pump fluence-dependent measurement as shown in Figure 2d. $\Delta R/R|_{t=0}$ shows clear linear dependence on pump fluence regardless of specific pump probe polarization. This suggests the measured amplitude variance of differential reflectivity as a function of pump polarization is purely a manifestation of anisotropic absorption of pump light.

To study the carrier densities dependent relaxation dynamics of $\Delta R/R$, we try to fit relaxation dynamics of $\Delta R/R$ thereafter. Exponential decay fittings would not only require at least two exponential terms but also a changing of ratio between different components with pump fluence (Supporting Information), this indicates nonlinear carrier density dependent recombination process. In view of this, we fit the entire set of data of the transient spectrum at different pump fluence by a simple model based on rate equation[28]

$$\frac{\mathrm{d}N_n(t)}{\mathrm{d}t} = G(t) - AN_n(t) - BN_n^2(t) - CN_n^3(t) \quad (2)$$

where $N_n(t)$ is the electron density, A (s^{-1}), B (cm^3/s), and C (cm^6/s) are the Schockley-Reed, direct electron–hole, and Auger recombination coefficients,[29] respectively. The generation rate, G ($\mathrm{cm}^{-3}\ \mathrm{s}^{-1}$), is proportional to the absorbed laser excitation q (W/cm^2), which is nonzero only during the pump pulse duration. Here we have made the assumption that $\Delta R/R$ has linear dependence on carrier density, and the absorption coefficient of the pump radiation remains independent of pump fluence, as expected for rapid relaxation of initially injected carrier and the bleaching of the sample remains linear with injected carrier density in the range of our experiment. Figure 2c shows the fit to the complete set of pump fluence dependent measurement with uniform A, B, and C parameters; the fitting results are plotted as solid lines. The relative contribution of Schockley-Reed, direct electron–hole, and Auger recombination to the carrier density relaxation is plotted in Supporting Information; Schockley-Reed and radiative recombination dominates the relaxation process, whereas the Auger process is negligible except during the initial stage after the pump excitation. We note this simple fitting is intended for qualitative evaluation of the relative proportion of lowest order recombination pathways, instead of quantitative determination of the actually dynamics.

DOI: 10.1021/acs.nanolett.5b01409
Nano Lett. 2015, 15, 4650–4656

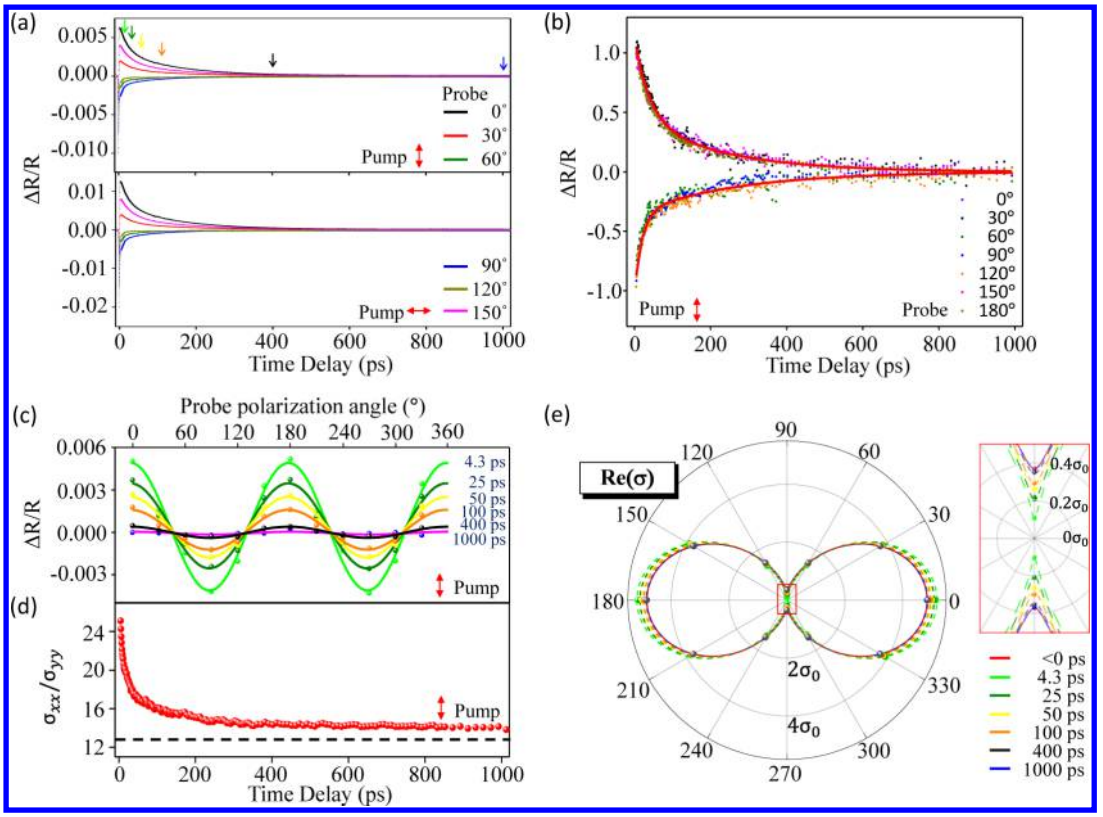

Figure 3. Probe polarization dependence of transient reflection spectra. (a) Probe polarization dependence of transient reflection spectrum with pump polarization fixed along 0° and 90°. (b) Normalized transient reflection spectrum (normalized with $\Delta R/R|_{t=4.5\ ps}$) with different probe polarization angle. (c) Transient reflection spectra with different probe polarization at fixed delays. The angle dependence is fit by function $\Delta R/R = a\cos^2\alpha + b\sin^2\alpha$. (d) Dynamic evolution of $\mathrm{Re}(\sigma_{xx})/\mathrm{Re}(\sigma_{yy})$ at different delays with pump polarized along 90°(without subtracting constant background). The black dash line marks value of $\mathrm{Re}(\sigma_{xx})/\mathrm{Re}(\sigma_{yy})$ in a sample prior to pumping. (e) Dynamical evolution of $\mathrm{Re}(\sigma)$ ellipse at different delays. $\Delta\mathrm{Re}(\sigma)$ is doubled for clarity. Inset: enlarged plot of area marked by red rectangle.

Figure 3a shows the probe polarization dependence of transient reflection spectra with pump polarization fixed along 0 and 90°. As the probe polarization rotates from 0 to 90°, the $\Delta R/R|_{t=0}$ stays negative, which corresponds to a pump-induced reflection decrease in both x- and y-axis of BP. The negative $\Delta R/R$ persists for several picoseconds, after which the value switches to positive for polarization angle close to x-axis. Further experiment shows the evolution of spectra as a function of probe polarization is qualitatively the same regardless of pump polarization. Consequently, we confirm that the transient reflection spectra depends weakly on pump polarization solely through anisotropic absorption. The material itself does not have any "memory" of pump polarization for the 200 fs experimental time resolution. As the initial negative $\Delta R/R$ around time zero is possibly due to highly nonequilibrium state, we normalize the peak negative/positive $\Delta R/R$ signal starting from ~4.5 ps to examine the relaxation dynamics at different probe polarizations. As shown in Figure 3b, the relaxation dynamics after the initial nonequilibrium state are independent of the probe polarization, which indicates the recombination and relaxation dynamics of photoexcited carriers are isotropic in BP.

The most remarkable observation is the sinusoidal oscillation of the $\Delta R/R$ as a function of probe polarization at fixed pump−probe delay, as shown in Figure 3c. This periodic oscillation is robust and persists for the whole decay process (~1 ns) except for the initial highly nonequilibrium state. This can be directly explained by the anisotropic response of optical conductivity. The measured $\Delta R/R$ can be converted to optical conductivity change $\Delta\sigma$ through the following equation assuming $\Delta\sigma \ll \sigma$, which is valid after the initial relaxation of highly excited states (see Supporting Information for deduction and the parameter range that the approximation is valid)

$$\begin{aligned}\frac{\Delta R}{R} &\approx \frac{4\sqrt{\varepsilon_1}\,\Delta\mathrm{Re}\,\sigma}{\varepsilon_0 c(\varepsilon_2-\varepsilon_1)} + \frac{8\sqrt{\varepsilon_1\varepsilon_2}\,(\Delta\mathrm{Im}\,\sigma)\mathrm{Im}\,\sigma}{\varepsilon_0^2 c^2(\varepsilon_2-\varepsilon_1)^2} \\ &\approx \frac{4\sqrt{\varepsilon_1}\,(\Delta\mathrm{Re}\,(\sigma_{xx})\cos^2\alpha_2 + \Delta\mathrm{Re}(\sigma_{yy})\sin^2\alpha_2)}{\varepsilon_0 c(\varepsilon_2-\varepsilon_1)} \\ &\quad + \frac{8\sqrt{\varepsilon_1\varepsilon_2}\,((\Delta\mathrm{Im}(\sigma_{xx})\cos^2\alpha_2 + \Delta\mathrm{Im}(\sigma_{yy})\sin^2\alpha_2))\mathrm{Im}\,\sigma}{\varepsilon_0^2 c^2(\varepsilon_2-\varepsilon_1)^2}\end{aligned} \tag{3}$$

The first and the second term of eq 3, respectively, account for the contribution of $\Delta\mathrm{Re}(\sigma)$ and $\Delta\mathrm{Im}(\sigma)$ (pump induced change of the real and imaginary parts of optical conductivity) to the transient reflection. In both terms, the transient reflection has sinusoidal dependence on the probe polarization angle α_2. Thus, from eq 3 to account for the sinusoidal oscillation observed in Figure 3b it follows immediately that $\Delta\sigma_{xx} \neq \Delta\sigma_{yy}$. This indicates $\Delta\sigma$ is anisotropic in BP although the relaxation dynamics are isotropic.

To interpret the dynamical response of BP under photoexcitation, we use a two-band model[7,30] to compute the optical conductivity of BP in quasi-equilibrium states, as a function of the effective temperature and the photo-generated excess

DOI: 10.1021/acs.nanolett.5b01409
Nano Lett. 2015, 15, 4650−4656

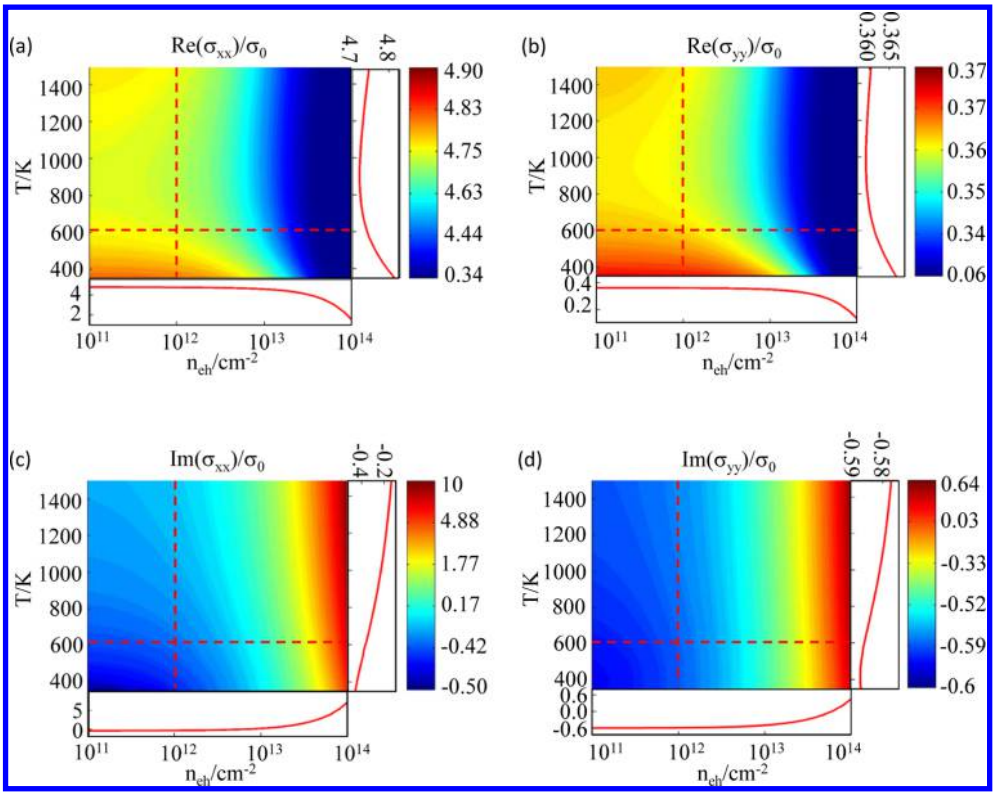

Figure 4. Computed dynamical conductivity. (a) $\mathrm{Re}(\sigma_{xx})/\sigma_0$ and (b) $\mathrm{Re}(\sigma_{yy})/\sigma_0$ as functions of photo-induced carrier density n_{eh} and quasi-equilibrium temperature T. The inset on the right (bottom) shows a cut at fix $n_{eh} = 10^{12}/\mathrm{cm}^2$ ($T = 600$ K) as marked by red dash line. (c) $\mathrm{Im}(\sigma_{xx})/\sigma_0$ and (d) $\mathrm{Im}(\sigma_{yy})/\sigma_0$ as a function of n_{eh} and T. The inset on the right (bottom) shows a cut at fix $n_{eh} = 10^{12}/\mathrm{cm}^2$ ($T = 600$ K) as marked by red dash line.

electron−hole density. The effective temperatures of electron and hole gases as well as their chemical potentials vary with time, as the density decreases through recombination. The real parts of the conductivity tensor are shown in Figure 4. The simulation gives $\mathrm{Re}(\sigma_x) = 4.84$ and $\mathrm{Re}(\sigma_y) = 0.37$ for unexcited state with initially hole doping of $1.03 \times 10^{13}/\mathrm{cm}^2$. Comparing with unexcited value, both $\Delta\ \mathrm{Re}(\sigma_{xx})$ and $\Delta\ \mathrm{Re}(\sigma_{yy})$ are negative in the parameter range that is plotted. The change of $\mathrm{Re}(\sigma)$ is primarily due to the Pauli blocking effect: the real part of conductivity, which mainly comes from interband transition, will be reduced due to the increased occupation of conduction and valence band of photoexcited carriers. We also observe the $\mathrm{Re}(\sigma)$ generally decreases with increasing photocarrier density; on the other hand, it shows a minimum when temperature increases at fixed density. This is expected from the effect of Pauli blocking when the carrier density is well below the energy scale of the probe transition. What is not taken into account in this model is the possible gap renormalization due to the electron hole interaction,[31] which could enhance the interband transition and thereby even overcompensate the Pauli Blocking.

The dynamical evolution of conductivity in parameter regions that is relevant to high field device can be extracted directly from experimentally measured transient reflection signal, independent of the above model. We note although both $\Delta\ \mathrm{Re}(\sigma)$ and $\Delta\ \mathrm{Im}(\sigma)$ as well as their respective contributions to the transient reflection vary throughout the relaxation processes, the contribution from $\Delta\ \mathrm{Re}(\sigma)$ usually dominates (see Figure S6 of Supporting Information). This is expected from eq 3, as the coefficient of the first term: $((4\sqrt{\varepsilon_1})/(\varepsilon_0 c(\varepsilon_2 - \varepsilon_1))) \sim (0.03/\sigma_0)$ is far larger than the coefficient of the second term: $((8(\varepsilon_1\varepsilon_2)^{1/2}\ \mathrm{Im}\ \sigma)/(\varepsilon_0{}^2 c^2(\varepsilon_2 - \varepsilon_1)^2)) \sim (0.001/\sigma_0) * ((\mathrm{Im}\ \sigma)/\sigma_0)$, taking $\sigma_0 = e^2/4\hbar$, $\varepsilon_1 = 1$, $\varepsilon_2 = 3.9$, $\varepsilon_0 c = (\sigma_0/0.023) = 43.5\ \sigma_0$, and Im $\sigma_x = -0.52\sigma_0$ and Im $\sigma_y = -0.60\ \sigma_0$ for native state of 25 nm thick BP sample (see Methods). Thus, in the limit $\Delta\mathrm{Re}\ (\sigma)$ is comparable with or larger than $\Delta\mathrm{Im}(\sigma)$, which is valid over the quasi-equilibrium state region after initial fast carrier cooling and recombination (as marked in Figure S6 of Supporting Information), the second term of eq 3 can be ignored. This simplification allows us to extract the dynamical evolution of $\mathrm{Re}(\sigma)$ through the simple relationship $((\Delta R)/R) \approx ((4\sqrt{\varepsilon_1}\Delta\mathrm{Re}\ \sigma)/\varepsilon_0 c(\varepsilon_2 - \varepsilon_1))$ from experimentally measured transient reflection signal, which is shown in Figure 3d,e. We observed conductivity ellipse is stretched ($\Delta\ \mathrm{Re}(\sigma_{xx}) > 0$ while $\Delta\ \mathrm{Re}(\sigma_{yy}) < 0$) due to photoexcitation of hot carriers, the stretch of conductivity ellipse persists over the subsequent relaxation process and gradually recovers as the photoexcited hot carriers relax and recombine.

The stretch of conductivity ellipse implies BP becomes more anisotropic under high field transport, which is equivalent to a quasi-equilibrium state of photoexcited carriers after initial relaxation and recombination processes. Here we want to clarify that the deduced conductivity ellipse closed to timezero (0 , 0.4, and possibly 4.3 ps delay) is dominated by either nonequilibrium state or highly excited quasi-equilibrium state. During this stage, the condition $\Delta\ \mathrm{Re}(\sigma) \perp \Delta\ \mathrm{Im}(\sigma)$ or $\Delta\ \mathrm{Re}(\sigma) > \Delta\ \mathrm{Im}(\sigma)$ is invalid, and the contribution of $\Delta\ \mathrm{Im}(\sigma)$ should not be ignored and may dominate the contribution to transient reflection signal. The dynamical evolution of conductivity is hard to justify from experiment in this region. However, if using typical energy of 0.1 eV as carriers accelerated to velocity saturation in high field device, this

DOI: 10.1021/acs.nanolett.5b01409
Nano Lett. 2015, 15, 4650−4656

energy is equivalent to 1000 K or photo-induced doping intensity of $3 \times 10^{13}/\mathrm{cm}^2$ if filling from the bottom of conduction band. This falls into the parameters region of the long transient reflection tails after the initial relaxation and recombination of photocarriers that is relevant to high speed device application.

Here we want to emphasize the enhanced anisotropic response is not relevant to pump polarization. Although the absorption of photon through direct interband transition in BP has linear dichroism, the memory of the BP of the excitation polarization is shorter than the ∼200 fs time resolution of our experiment. The nonuniform distribution of carrier in k space is erased possibly due to fast carrier−carrier scattering process. The isotropic relaxation along any polarization directions thereafter may also share the same origin as above: the fast carrier−carrier scattering mediates the carrier distribution in k space in sub-200 fs time scale, this fast modification of carrier distribution gives isotropic relaxation/recombination behavior magnified in the transient reflection spectroscopy, although the carrier phonon scattering and carrier recombination are possibly highly anisotropic.

It should be remarked that the computed change in the real part of the conductivity in the x-direction is ostensibly negative, although the experimentally inferred $\Delta\ \mathrm{Re}(\sigma_{xx}) > 0$. There are a few sources that can in principle cause this discrepancy from the modeling perspective. First, the computed $\Delta\ \mathrm{Re}(\sigma_{xx})$ is negative primarily because of the Pauli Blocking. Second, the gap renormalization due to the many body effect, as mentioned earlier, could compensate or even over compensate the Pauli blocking. Third, there could be multiband physics that are beyond the scope of this simple two-band model. These, however, make the microscopic origin of the enhancement of electronic anisotropy all the more interesting. Further theoretical analysis is warranted to clarify the dynamical processes of photocarriers as well as change in the electronic structure in the pump−probe experimental setting.

This experimental work provides interesting device physics toward understanding angle-sensitive operation behavior of various BP-based optoelectronic devices when light illumination is involved, such as a photodetector, remote sensing device, and optical modulator or any BP-based devices running in high field transport limit. The numerical simulations provide general support for the observed dynamical enhancement of anisotropy. It should be remarked that the sign of the conductivity in some region does not agree with the experimental inference, which could be a result of band gap renormalization and/or dynamical effects beyond linear-response and warrant further systematic studies. On top of BP's extraordinary properties of high mobility and thickness-dependent bandgap suitable for mid-infrared wavelength, a spectral range that was previously difficult to access, the preservation, and enhancement of anisotropic response and linear dichroism under excited state make BP an ideal material, distinguished from conventional materials and approaches for angle sensitive devices, capable of working in high-field applications such as ballistic transistor and high speed polarization sensors where both high mobility and anisotropy are desired. As a new member of 2D family, BP also shares the advantage of easy integration with other 2D materials, facilitating its application for multifunctional integrated electronics, and photonics circuits based on multiple 2D materials.

Methods. *Sample Preparation.* Thin BP flakes are obtained by mechanical exfoliation a synthesized bulk BP crystal on 285 nm SiO2 substrate. Single crystals of BP are grown by a chemical vapor transport method as previously described.[32] Red phosphorus (500 mg), AuSn (364 mg), and SnI4 (10 mg) are sealed in an evacuated quartz ampule of 12 cm long. The end with the charges of the ampule is placed horizontally at the center of a single zone tube furnace. The ampule is slowly heated up to 873 K within 10 h and kept at this temperature for 24 h. Then the ampule is cooled to 773 K at a rate of 40 K/h. Single crystals of BP crystallized in flake-like form with the sizes larger than 1 cm are obtained at the cold end of the ampule.

Transient Reflection Spectroscopy. An infrared optical parametric amplifier (OPA) pumped by a 60 fs, 250 kHz Ti: Sapphire regenerative amplifier (RegA) is used in the transient reflection measurement. The idler from OPA at 1940 nm (∼150 fs) is used as probe and the dispersion-compensated residual 800 nm of the OPA is used as the pump. Both pump and probe pulses are linearly polarized and two half-wave plates are used to alter their polarization angle, respectively. A 40× reflective objective lens is used to focus the copropagating pump probe spots onto the sample that is cooled in a liquid nitrogen-cooled cryostat for temperature control. The reflected probe is collected by the same objective lens and routed through a monochromator followed by an InGaAs photodetector. The detected probe reflection is read by lock-in amplifier referenced to 5.7 kHz mechanically chopped pump. The probe spot size is estimated to be 4 μm with a pump spot size slightly larger. The pump excited carrier density is estimated to be around $1.3 \times 10^{15}/\mathrm{cm}^2$ unless in a pump fluence-dependent measurement.

Two-band Model Simulation. We use the two-band tight binding (TB) model as in refs 7 and 30

$$H_j(\mathbf{k}) = \begin{bmatrix} E_{cj} + \eta_c k_x^2 + \nu_c k_y^2 & \gamma k_x + \beta k_y^2 \\ \gamma k_x + \beta k_y^2 & E_{vj} - \eta_v k_x^2 - \nu_v k_y^2 \end{bmatrix}$$

where j is the subband index, $\eta_c = \eta_v = \hbar^2/0.4m_0$, $\nu_c = \hbar^2/1.4m_0$, $\nu_v = \hbar^2/2.0m_0$, $\gamma = 4a/\pi$ eV, $\beta = 6.2\ a^2/\pi^2$ eV, m_0 is the free electron mass, $2a = 4.46$ Å is the lattice constant along the x-direction. Because the sample is 25 nm thick, the energy dispersion of the z-direction should be considered. By the envelope function method, $E_{cj} = j^2\pi^2\hbar^2/m_z^c d^2$, $E_{vj} = -\delta\ (d) - j^2\pi^2\hbar^2/2m_z^v d^2$, where $m_z^c = 0.2m_0$, $m_z^v = 0.4m_0$, $d = 25$ nm is the sample thickness, and $\delta(d) = 0.3$ eV is the band gap.

The conductivity corresponding to the incident light with frequency ω is given by the Kubo's formula. The scattering time is set to the equivalent of 0.01 eV, following Low et al.[7,30] For equilibrium states, the chemical potentials of electrons and holes are equal: $\mu_e = \mu_h$. However, when the photoexcited electrons and holes settle down to a quasi-equilibrium state, their chemical potentials are in general unequal: $\mu_e \neq \mu_h$. μ_e and μ_h are determined by the photocarrier density and their quasi-equilibrium temperature. For all calculations, the BP is hole-doped with a hole density of $10^{13}\ \mathrm{cm}^{-2}$.

■ ASSOCIATED CONTENT

Ⓢ Supporting Information

Deduction of absorption coefficient and transient reflection, biexponential and rate equation fitting of pump power dependence, polarization and temperature dependence of transient reflection background, and computational details. The Supporting Information is available free of charge on the

DOI: 10.1021/acs.nanolett.5b01409
Nano Lett. 2015, 15, 4650−4656

ACS Publications website at DOI: 10.1021/acs.nanolett.5b01409.

AUTHOR INFORMATION

Corresponding Authors

*E-mail: jfeng11@pku.edu.cn.
*E-mail: sundong@pku.edu.cn.

Notes

The authors declare no competing financial interest.

ACKNOWLEDGMENTS

This project has been supported by the National Basic Research Program of China (973 Grants 2012CB921300, 2013CB921900, and 2014CB920900), the National Natural Science Foundation of China (NSFC Grants 11274015 and 11174009), the Recruitment Program of Global Experts, Beijing Natural Science Foundation (Grant 4142024) and the Specialized Research Fund for the Doctoral Program of Higher Education of China (Grant 20120001110066).

REFERENCES

(1) Xia, F. N.; Wang, H.; Xiao, D.; Dubey, M.; Ramasubramaniam, A. *Nat. Photonics* **2014**, *8*, 899−907.
(2) Xia, F. N.; Wang, H.; Jia, Y. C. *Nat. Commun.* **2014**, *5*, 4458.
(3) Akahama, Y.; Endo, S.; Narita, S. *J. Phys. Soc. Jpn.* **1983**, *52*, 2148−2155.
(4) Liu, H.; Neal, A. T.; Zhu, Z.; Luo, Z.; Xu, X. F.; Tomanek, D.; Ye, P. D. *ACS Nano* **2014**, *8*, 4033−4041.
(5) Qiao, J.; Kong, X.; Hu, Z.-X.; Yang, F.; Ji, W. *Nat. Commun.* **2014**, *5*, 4475.
(6) Wang, X. M; Jones; Aaron, M.; Seyler; Kyle, L.; Tran; Vy; Jia, Y. C; Zhao, H.; Wang, H.; Yang, L.; Xu, X. D.; Xia, F. N. *Nat. Nanotechnol.* **2015**, *10*, 517−521.
(7) Low, T.; Rodin, A. S.; Carvalho, A.; Jiang, Y. J.; Wang, H.; Xia, F. N.; Neto, A. H. C. *Phys. Rev. B* **2014**, *90*, 075434.
(8) Tran, V.; Soklaski, R.; Liang, Y. F.; Yang, L. *Phys. Rev. B* **2014**, *89*, 235319.
(9) Li, L. K.; Yu, Y. J.; Ye, G. J.; Ge, Q. Q.; Ou, X. D.; Wu, H.; Feng, D. L.; Chen, X. H.; Zhang, Y. B. *Nat. Nanotechnol.* **2014**, *9*, 372−377.
(10) Du, Y. C.; Liu, H.; Deng, Y. X.; Ye, P. D. *ACS Nano* **2014**, *8*, 10035−10042.
(11) Wang, H.; Wang, X. M.; Xia, F. N.; Wang, L. H.; Jiang, H.; Xia, Q. F.; Chin, M. L.; Dubey, M.; Han, S. J. *Nano Lett.* **2014**, *14*, 6424−6429.
(12) Xiang, D.; Han, C.; Wu, J.; Zhong, S.; Liu, Y.; Lin, J.; Zhang, X.-A.; Ping, H. W.; Özyilmaz, B.; Neto, A. H. C.; et al. *Nat. Commun.* **2015**, *6*, 6485.
(13) Zhu, W.; Yogeesh, M. N.; Yang, S.; Aldave, S. H.; Kim, J.-S.; Sonde, S.; Tao, L.; Lu, N.; Akinwande, D. *Nano Lett.* **2015**, *15*, 1883−1890.
(14) Baba, M.; Takeda, Y.; Shibata, K.; Ikeda, T.; Morita, A. *Jpn. J. Appl. Phys.* **1989**, *2* (28), L2104−L2106.
(15) Buscema, M.; Groenendijk, D. J.; Blanter, S. I.; Steele, G. A.; van der Zant, H. S. J.; Castellanos-Gomez, A. *Nano Lett.* **2014**, *14*, 3347−3352.
(16) Buscema, M.; Groenendijk, D. J.; Steele, G. A.; van der Zant, H. S. J.; Castellanos-Gomez, A. *Nat. Commun.* **2014**, *5*, 4651.
(17) Engel, M.; Steiner, M.; Avouris, P. *Nano Lett.* **2014**, *14*, 6414−6417.
(18) Youngblood, N.; Chen, C.; Koester, S. J.; Li, M. *Nat. Photon.* **2015**, *9*, 247−252.
(19) Yuan, H.; Liu, X.; Afshinmanesh, F.; Li, W.; Xu, G.; Sun, J.; Lian, B.; Ye, G.; Hikita, Y.; Shen, Z. *Nat. Nanotechnol.* **2015**, DOI: 10.1038/nnano.2015.112.
(20) Warschauer, D. *J. Appl. Phys.* **1963**, *34*, 1853−1860.
(21) Fei, R. X.; Yang, L. *Nano Lett.* **2014**, *14*, 2884−2889.
(22) Qin, G.; Yan, Q.-B.; Qin, Z.; Yue, S.-Y.; Hu, M.; Su, G. *Phys. Chem. Chem. Phys.* **2015**, *17*, 4854−4858.
(23) Sun, D.; Wu, Z.-K.; Divin, C.; Li, X.; Berger, C.; de Heer, W. A.; First, P. N.; Norris, T. B. *Phys. Rev. Lett.* **2008**, *101*, 157402.
(24) Yao, Z.; Kane, C. L.; Dekker, C. *Phys. Rev. Lett.* **2000**, *84*, 2941−2944.
(25) Sinitsky, D.; Assaderaghi, F.; Hu, C. M.; Bokor, J. *IEEE Electron Device Lett.* **1997**, *18*, 54−56.
(26) Shishir, R. S.; Ferry, D. K.; Goodnick, S. M. *J. Phys.: Conference Series* **2009**, *193*, 012118.
(27) Morita, A. *Appl. Phys. A* **1986**, *39*, 227−242.
(28) Shen, Y. C.; Mueller, G. O.; Watanabe, S.; Gardner, N. F.; Munkholm, A.; Krames, M. R. *Appl. Phys. Lett.* **2007**, *91*, 141101.
(29) Findlay, P. C.; Pidgeon, C. R.; Kotitschke, R.; Hollingworth, A.; Murdin, B. N.; Langerak, C.; van der Meer, A.; Ciesla, C. M.; Oswald, J.; Homer, A.; et al. *Phys. Rev. B* **1998**, *58*, 12908−12915.
(30) Low, T.; Roldan, R.; Wang, H.; Xia, F. N.; Avouris, P.; Moreno, L. M.; Guinea, F. *Phys. Rev. Lett.* **2014**, *113*, 106802.
(31) Hwang, E. H.; Das Sarma, S. *Phys. Rev. B* **1998**, *58*, R1738−R1741.
(32) Nilges, T.; Kersting, M.; Pfeifer, T. *J. Solid State Chem.* **2008**, *181*, 1707−1711.

DOI: 10.1021/acs.nanolett.5b01409
Nano Lett. 2015, 15, 4650−4656